

# 利用酵素與奈米微粒之生物分子交互作用調控催化活性

研究生:吳中書

指導教授:柯富祥 教授

國立交通大學材料科學與工程學系奈米科技 博士班

## 摘 要

蛋白質表面的修飾與辨識在生物科學領域裡常用來探討蛋白質與蛋白質交互作用及酵素催化活性，在本篇研究中，我們利用奈米微粒本身對生物分子的作用力將酵素修飾於粒子的表面並探討其酵素特性，我們發現酵素固定於奈米微粒上其活性會有顯著性的增加，利用動力學及熱力學實驗分析此具有酵素催化功能的奈米粒子，我們能夠解釋和預測其反應行為並了解此增強活性之機制。由於奈米微粒與生物分子的尺寸互相匹配，因此奈米粒子常用於酵素固定化之基材，在接下來的研究中，我們嘗試將酵素修飾於不同大小之奈米微粒，我們發現當固定於較小的粒子時，其反應速率明顯增強，經由進一步的動力學實驗發現，此奈米微粒的粒徑大小會影響此酵素與反應基質之親和力以至於改變其催化活性與行為。為了解釋奈米微粒在反應過程所扮演之角色，我們提出一套理論解釋此現象，由於不同大小之奈米微粒有不同的立體障礙效應，其碰撞機率會隨著粒徑變小而增加，因此對催化速率產生影響。本項研究包含了實驗數據以及理論探討，並詳細地解釋奈米粒子與酵素之間的交互作用，說明奈米微粒對於酵素催化行為所扮演的角色。在生物體中酵素活性的調控與生長、合成和代謝等反應直接相關，利用奈米微粒調控催化活性的能力對於日後在奈米生物領域上的發展有所貢獻。

# Regulation of Catalytic Activity *via* the Biomolecular Interactions Based on Enzyme–Nanoparticle Conjugates

Student : Chung-Shu Wu

Advisor : Prof. Fu-Hsiang Ko

Department of Materials Science and Engineering  
National Chiao Tung University

## Abstract

Protein surface recognition provides an appealing tool to regulate protein–protein interactions and enzymatic activities in the field of biological science. We are interested in using nanoparticle (NP) to bind enzyme surfaces through multivalent interactions and then engineer the protein properties. In this study, we have investigated the activity of the enzyme–NP conjugates and demonstrated that adsorbing enzyme onto NPs significantly increased its enzymatic activity. We ascribe this event of the enzymatic reactions by kinetic and thermodynamic studies, which provide a way of understanding and predicting the catalytic behaviors of the enzyme–functionalized NPs. In addition, NPs are excellent systems for modeling enzymes' surfaces because they can be readily fabricated on size scales comparable with those of their biomolecular targets. Therefore, we were curious to study whether varying the dimensions of the NPs would affect their catalytic reactions. We have developed a series of kinetic experiments to systematically analyze the NP size–dependent enzymatic activities, and have developed a model to explain the phenomenon. Kinetic studies revealed that association of enzyme with NPs did not influence the turnover number, but smaller NPs did promote the catalytic efficiency of enzyme by increasing its kinetic affinity. A shielding model, based on diffusion–collision theory, explains the correlation between the size effects and the kinetic responses of the enzyme–NP conjugates. This size-effect model provides chemical and physical meaning, leading to the observed substrate specificities and catalytic constants. From the combined kinetic and theoretical investigation of enzyme bound to NPs, we found that these conjugates acted as a controllable and efficient factor for modulating the activity of the enzyme. In nature, controllable modulation of enzyme activity is a potent means of regulating several cellular processes (e.g., signal transduction, biosynthesis, metabolism). The modulation of biocatalytic behavior is an attractive feature for exploitation in the field of nanobiotechnology.

# Acknowledgment

碩士班口試時我被問的第一個問題：『中書，怎麼致謝內容都沒有提到人名，你怎麼能夠保證十年、二十年之後你還會記得?』。其實當下我想回答：『會被我忘記的人，怎麼還需要感謝?』。正如同碩士論文致謝裡的一段話：『該感謝的人一個都不能少，不該感謝的人一個都不能多，不然就失去了這一頁的意義~』。然而，現在，三年過去了，值得慶幸的是我依舊記得他們，此頁獻給那些曾經真正在乎我、了解我，而我該感謝的人。

最近常常聽到的一句話：『哇!中書，你今年就可以畢業了喔!』。接下來就是一些，你很優秀、很厲害、很順利之類的客氣話~然而每當這些話語過後，我都會試想這個人到底了解我多少。我想，如果是真的認識我的人，應該不會對我說這些客套話吧!這三年，我只是很認真的去做每件事，我不優秀但我願意花時間去學；我不厲害但我可以犧牲睡眠時間把事情盡快完成；投稿不順利但我會在最短的時間內修改完回覆給教授。真正認識我的人，我做的一切他們都看在眼中，我的付出我的努力，他們不會用優秀、厲害、順利，這樣的字眼帶過，而這樣的人，才有資格放在這頁裡，如果把他們的名字也跟別人列在一起，那是否對我該感謝的人也太不尊重了些?

『肩膀，要夠大』，這是一位學長曾經跟我說的話，他是我在研究領域上的啟蒙者，很多好(或不好)的觀念，都是他影響了我，而我也繼續傳承下去。這句話涵義很深，在博士班生涯中我已體會箇中滋味，在未來的旅程中隨著年齡的增長，角色和責任會越來越多，學習如何『扛』下，我還需要更多的學習和歷練；『馬步站穩，眼光放遠』，這是另一位影響我很深的學長在信件往返中所送我的話，這句話代表他做人做事的準則，講求把『基本功』練好，著眼未來就會有好的發展空間。他是我人生道路上的典範，也許是因為人生經驗相差太多，往往跟他討論時我能夠得到不同角度分析事情的看法，雖然很遺憾跟他學習的時間並不多，但對我卻很受用；對指導教授的感謝，相信這三年來我已用行動表達了我的感謝之意，有幸在教授的門下盡情發揮，著實讓我學習、體驗到不少事物，也因為有你，我們大家才有相處在一起的機會。

在這頁的最後，獻上最大的感謝之意給我的家人，包括：媽媽、哥哥以及女朋友，你們是我的避風港，當我情緒低落、失意的時候提供一個溫暖、無私的空間，因為是我的家人，任性的一面才能在你們面前表露，所以這三年給予了你們莫大的壓力，但也正因為你們，我才能很優秀、很厲害、很順利的拿到這該屬於我們一家人的一博士學位。

# Contents

<b>Chapter 1 Overview</b>	<b>1</b>
1.1 General Introduction	1
1.2 Nanobiotechnology	2
1.3 Applications of Nanoparticles in Biology	5
1.4 Nanoparticle–Biomolecule Interactions	10
1.5 Surface Interaction of Biomolecules with Gold Nanoparticles	12
<b>Chapter 2 Literatures Review</b>	<b>15</b>
2.1 General Introduction: Applications of AuNPs in Nanobiotechnology	15
2.1.1 Oligonucleotide-Modified AuNPs	16
2.1.2 Enzyme-Modified AuNPs	22
2.1.3 Effect of Nanoparticle Size on Enzyme Activity	27
2.1.4 Summary	29
2.2 Lipases	30
2.2.1 Interfacial Enzymes with Attractive Applications	30
2.2.2 Structure and Reaction Mechanism of Esterase	31
<b>Chapter 3 Experiments</b>	<b>33</b>
3.1 General Introduction	33
3.1.1 General Chemicals	33
3.1.2 Synthesis of Colloidal AuNPs	34
3.1.3 Immobilization of AuNPs on Silicon Wafer	34
3.1.4 Activity Assay of Enzyme–AuNP Conjugates System	34
3.2 Instruments	35
3.3 Experimental Methods	36

3.3.1	Synthesis and Characterization of Colloidal AuNPs	36
3.3.2	Immobilization and Observation of AuNPs on Silicon Wafer	37
3.3.3	Preparation of CRL–AuNP Conjugates	38
3.3.4	Activity Assay of Free and AuNP-Bound CRL Systems	39
3.3.5	Michaelis–Menten Kinetics	40
<b>Chapter 4</b>	<b>An Enzymatic Kinetics Investigation into the Significantly Enhanced Activity through the Linker-Free Gold Nanoparticle Pathway</b>	<b>41</b>
4.1	Background	41
4.2	Results and Discussion	43
4.2.1	Mechanism of the Catalytic Reaction by the AuNP-Bound Lipase	43
4.2.2	Observation of AuNPs on Silicon Wafer	45
4.2.3	Determining the Immobilization of Enzyme Capped AuNPs on Silicon Wafer	47
4.2.4	Determining the Enzyme Coverage of AuNPs with Lipase	49
4.2.5	Activity Assays of the Free and AuNPs-Bound Lipase	57
4.2.6	Effect of AuNPs Concentration on Catalytic Activity	58
4.2.7	Kinetic and Thermodynamic Investigations of Enzyme-Functionalized AuNPs	59
4.3	Conclusions	62
<b>Chapter 5</b>	<b>Size-Modulated Catalytic Activity of Enzyme–Nanoparticle Conjugates: A Combined Kinetic and Theoretical Study</b>	<b>63</b>
5.1	Background	63
5.2	Results and Discussion	66
5.2.1	Particle Size Distribution and Mean Diameter of AuNPs	66
5.2.2	Apparent Dissociation Constant and Enzyme Coverage—Analysis and Definition	69



5.2.3	Preparation of CRL–AuNP Conjugates	72
5.2.4	Activity Assay of CRL–AuNP Conjugated Systems	75
5.2.5	Kinetic Investigation of CRL–AuNP Conjugates	77
5.2.6	Collision Model with a Shielding Factor	81
5.2.7	Diffusion–Collision Theory for Enzyme–NP Conjugates	84
5.2.8	Effect of Nanoparticle Size on the Catalytic Activity: Theoretical Approach	86
5.3	Conclusions	88
<b>Appendix</b>		<b>89</b>
A.1	A Surface Limited Model for the Evaluation of Immobilized Enzyme on Planar Surface	89
	Experimental Section	89
	Theoretical Considerations	94
	Results and Discussion	98
A.2	Dimension of the Enzyme CRL	102
A.3	Dimension of the Substrate <i>p</i> NPP	103
<b>Curriculum Vitae</b>		<b>104</b>
C.1	Education	104
C.2	Skills	104
C.3	Publication List	104
C.4	Conferences	106
<b>Global Medical Discovery</b>		<b>108</b>
<b>References and Bibliography</b>		<b>109</b>

# List of Tables

<b>Table 1.1</b> .....	<b>9</b>
Characteristics, ligands and representative applications for various metal and semiconductor materials	
<b>Table 1.2</b> .....	<b>11</b>
Strategies for labeling a specific residue that involve direct linkage to the NP core	
<b>Table 2.1</b> .....	<b>18</b>
Melting temperatures and enthalpies for different sized nanoparticles in the solution aggregate system	
<b>Table 2.2</b> .....	<b>18</b>
Melting temperatures and enthalpies for different surface densities of probe oligonucleotides on the nanoparticles in the solution aggregate system	
<b>Table 5.1</b> .....	<b>67</b>
Various concentrations of trisodium citrate (1 mL) added to HAuCl <sub>4</sub> solution (10 mL) and the maximum absorbance related with the differently sized AuNPs	
<b>Table 5.2</b> .....	<b>72</b>
Supernatant activity tests <sup>a</sup> during removal of unbound CRL from AuNP samples (mean sizes: 13.1, 25.2, 37.5, 50.8, and 69.6 nm, respectively) using centrifugation	
<b>Table 5.3</b> .....	<b>74</b>
Average values for the number of proteins per particle and surface density (coverage) for each particle size	
<b>Table 5.4</b> .....	<b>79</b>
Experiment-determined catalytic parameters of turnover numbers ( $k_{cat}$ ), Michaelis constants ( $K_m$ ), and specificity constants ( $k_{cat}/K_m$ ) for the free CRL, the CRL–AuNP conjugates and planar surface–immobilized CRL systems	
<b>Table 5.5</b> .....	<b>87</b>
Theoretical parameters <sup>a</sup> for the CRL–AuNP conjugates and planar surface–immobilized CRL systems	

# List of Figures

## Chapter 1

**Figure 1.1.....3**

Chemistry is the central science for the development of applied disciplines such as materials research and biotechnology. Materials science, which is based on classic chemical research fields and engineering technologies, has led to enormous advances in tailoring advanced modern materials.

**Figure 1.2.....3**

A gap currently exists in the engineering of small-scale devices. Whereas conventional top-down processes hardly allow the production of structures smaller than about 100–200 nm, the limits of regular bottom-up processes are in the range of about 2–5 nm.

**Figure 1.3.....5**

Sizes, shapes, and compositions of metal nanoparticles can be systematically varied to produce novel materials with distinct light-scattering properties.

**Figure 1.4.....7**

Chemistry is the central science for the development of applied disciplines such as materials research and biotechnology. Nanoparticles, which is based on classic chemical research fields and engineering technologies, has led to enormous advances in tailoring advanced nanobiotechnology.

**Figure 1.5.....10**

Integrated nanoparticle–biomolecule hybrid systems.

**Figure 1.6.....14**

Schematic representation of the formation of gold nanoparticle probes.



## Chapter 2

**Figure 2.1.....17**

In the presence of complementary target DNA, oligonucleotide-functionalized gold nanoparticles will aggregate (A), resulting in a change of solution color from red to blue (B). The aggregation process can be monitored using UV–Vis spectroscopy or simply by spotting the solution on a silica support (C).

**Figure 2.2.....19**

The diagram of using of AuNP–oligonucleotide complexes as intracellular gene regulation agents for the control of protein expression in cells.

**Figure 2.3.....19**

Confocal fluorescence microscopy images showing EGFP knockdown. (A) Untreated control cells (upper left, Cy5.5 emission, 706 to 717 nm; upper right, EGFP emission, 500 to 550 nm; lower left, transmission image of cells; lower right, composite overlay of all three channels) showed a significant amount of emission throughout the cell. (B) 1  $\mu$ m sectioning images of control cells. (C and D) Cells treated with antisense particles showed a decrease in the amount of EGFP emission.

**Figure 2.4.....21**

(a) Nanoparticles functionalized with a recognition sequence are hybridized with a short complementary Cy5 labeled reporter strand, which is capable of being displaced by the target. (b) Fluorescence spectra of nano-flares alone (green), in the presence of target (red), and in the presence of noncomplementary sequence (blue). (c) Oligonucleotide sequences.

**Figure 2.5.....22**

Aptamer nano-flares are gold nanoparticles functionalized with thiol-terminated aptamer sequences hybridized to a short complementary Cy5-labeled reporter strand. The reporter is capable of being displaced by a conformation change in the aptamer that is induced by the target molecule.

**Figure 2.6.....23**

(a) Space-filling model of ChT. Surface binding of the proteins by anionic MMPCs focuses on the ring of cationic residues situated around the active site, functionally significant residues are noted. (b) Relative sizes of ChT and MMPC **1**. (c) Anionic MMPCs **1** and **2** and cationic control **3**.

<b>Figure 2.7</b> .....	<b>25</b>
(a) Space-filling model of ChT. Active site (yellow) is surrounded by a ring of cationic residues (blue). (b) Amphiphilic MMPCs with anionic functional groups (carboxylate groups; red) in their terminals can interact with ChT <i>via</i> electrostatic complementarity. (c) Four derivatives of trimethylamine-functionalized surfactant used for surface modification of MMPC anionic monolayer. (d) Monolayer composition of AuCOOH as an effective inhibitor of ChT activity.	
<b>Figure 2.8</b> .....	<b>25</b>
Proposed mechanism of ChT rescue. The surfactants with thiol MMPC <b>5</b> and alcohol MMPC <b>6</b> at their terminals have the ability to elicit ChT release by interaction or partial displacement of the anionic monolayer. C <sub>11</sub> alkane MMPC <b>4</b> forms a bilayer-like structure, causing release of the ChT (red = anionic; blue = cationic).	
<b>Figure 2.9</b> .....	<b>26</b>
(a) Molecular structure of $\alpha$ -chymotrypsin (ChT). (b) Chemical structure of amino-acid-functionalized gold nanoparticles and substrates. (c) Schematic representation of monolayer-controlled diffusion of the substrate into and the product away from the active pocket of nanoparticles-bound ChT.	
<b>Figure 2.10</b> .....	<b>27</b>
a) The design of functionalized, cationic AuNPs as a template for peptide ligation. b) Helicity of E1E2, E1, and E2 with added cationic AuNPs. c) Initial rate of E1E2 <i>versus</i> the concentration of AuNPs.	
<b>Figure 2.11</b> .....	<b>28</b>
Schematic of lysozyme adsorption on nanoparticles with different sizes. Stronger protein particle interactions exist in the case of larger nanoparticles, resulting in more protein unfolding and less enzymatic activity.	
<b>Figure 2.12</b> .....	<b>31</b>
Structure of lipase in closed (A, C) and open form (B, D). A and B (side view): the catalytic triad (yellow) and secondary structure elements showing the $\alpha/\beta$ -hydrolase fold common to all lipases. Upon opening of the lid, the catalytic triad (yellow) becomes accessible (D).	
<b>Figure 2.13</b> .....	<b>32</b>
Catalytic mechanism of lipases based on a “catalytic triad” of serine (nucleophile), histidine, and aspartate or glutamate.	

## Chapter 3

**Figure 3.1**.....37

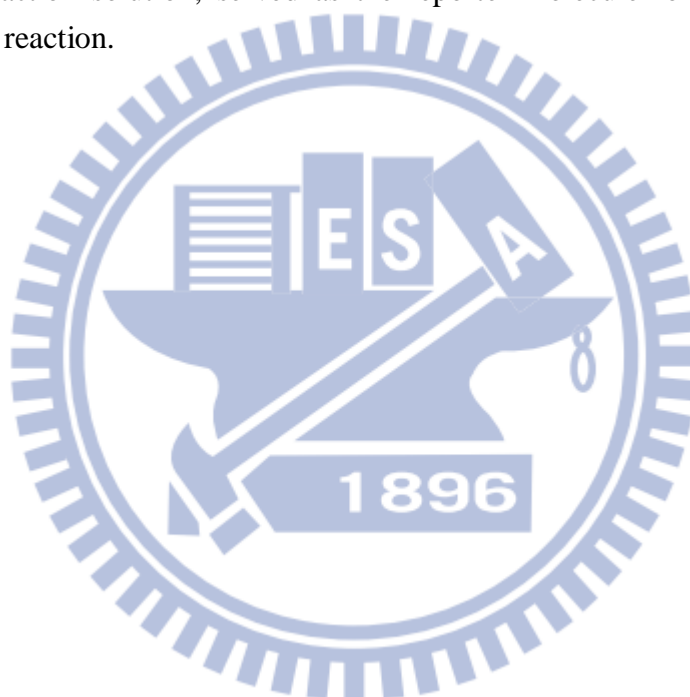
Schematic steps for the synthesis of differently sized gold nanoparticles.

**Figure 3.2**.....38

Self-assembly steps for the immobilization of gold nanoparticles onto silicon oxide surface.

**Figure 3.3**.....39

CRL-catalyzed hydrolysis of *p*NPP. The product, *p*NP, which provided strong absorption at 405 nm in the reaction solution, served as the reporter molecule for the progress of the enzyme-catalyzed reaction.



## Chapter 4

- Figure 4.1**.....42  
Schematic representation of the mechanism of catalysis of enzyme-functionalized AuNPs. Color scheme: AuNPs, gold; enzyme, green; first product, pink; second product, blue.
- Figure 4.2**.....44  
Mechanism of the catalytic reaction mediated by the enzyme-functionalized AuNPs.
- Figure 4.3**.....46  
a) SEM image of AuNPs immobilized onto a silicon dioxide surface through an MPTMS linker. b) Particle size distribution of the AuNPs present in the SEM image, analyzed using a personal computer and Image-Pro Plus software.
- Figure 4.4**.....47  
Self-assembly steps for enzyme-functionalized capped gold nanoparticles onto silicon oxide surface.
- Figure 4.5**.....48  
XPS spectra of AuNPs measured in the presence (blue) and absence (red) of the enzyme on the silicon dioxide surface.
- Figure 4.6**.....48  
FTIR spectra of enzyme capped gold nanoparticles on the silicon wafer.
- Figure 4.7**.....50  
a) Determining the degree of enzyme immobilization on non-aggregated AuNPs. UV–Vis absorption spectra of AuNPs in DI water (black), AuNPs in NaCl solution (red), enzyme-capped AuNPs in DI water (green), and enzyme-capped AuNPs after adding NaCl solution (blue). b) Photographic image of solutions of (A) AuNPs in DI water, (B) AuNPs in NaCl solution, (C) AuNPs capped with lipase in DI water, and (D) AuNP-bound lipase in DI water after adding NaCl solution. The variation in color allowed discrimination between the aggregated and non-aggregated AuNPs in aqueous solution; i.e., a distinguishable color change from red (A, C, and D) to blue (B) occurred upon aggregation.
- Figure 4.8**.....52  
a) The diagram of determining the optimal immobilization of lipase-functionalized on gold

nanoparticles. Variation in b) photographic image and c) UV–Vis absorbance spectra of the AuNPs (2.2 nM) at different concentrations of enzyme after adding NaCl solution.

**Figure 4.9**.....53

Plots of changes in the time-dependent absorption ratio (A620/A520) in the presence of varying concentration of lipase 1)  $93.75 \times 10^{-9}$  M, 2)  $18.75 \times 10^{-8}$  M, 3)  $22.5 \times 10^{-8}$  M, 4)  $30 \times 10^{-8}$  M, 5)  $37.5 \times 10^{-8}$  M, 6)  $0.45 \times 10^{-6}$  M, 7)  $0.75 \times 10^{-6}$  M, 8)  $1.5 \times 10^{-6}$  M, 9)  $2.4 \times 10^{-6}$  M after the addition of salt solution.

**Figure 4.10**.....54

Plot of the absorption ratio (A520/A620) in equilibrium *versus* the lipase concentration.

**Figure 4.11**.....57

a) Product (*p*NP) formation over time in the catalytic reactions of various concentrations of AuNP-bound (solid) and free lipase (hollow) solutions monitored at 405 nm. b) Initial velocities of *p*NP from *p*NPP plotted as a function of the concentration of the free enzyme (●) and the enzyme-capped AuNPs (○).

**Figure 4.12**.....58

Initial rate of *p*NP production *versus* the concentration of AuNPs. Conditions : pH 7.4, 30°C, [enzyme] = 100 nM, [substrate] = 22.22 μM.

**Figure 4.13**.....61

Michaelis–Menten plots for the hydrolyses of *p*NPP mediated by the free enzyme (blue) and enzyme-capped AuNPs (red).

**Figure 4.14**.....61

Arrhenius plots of ln(absorbance) *versus* the reciprocal of absolute temperature for the free (blue, inset) and AuNP-bound (red) lipase. The activity was measured for reaction mixtures containing 0.1 μM enzyme at pH 7.4.

## Chapter 5

- Figure 5.1**.....65  
Schematic representation of the preparation of CRL–AuNP conjugates that modulate the activity of the enzyme, and a cartoon of the shielding model.
- Figure 5.2**.....67  
UV–Vis spectrum of aqueous AuNPs with the diameters of 13.1, 25.2, 37.5, 50.8 and 69.6 nm.
- Figure 5.3**.....68  
SEM images (JEOL JSM-6700F electron microscope operated at 20 kV) of AuNPs with mean diameters of (a) 13.1, (b) 25.2, (c) 37.5, (d) 50.8, and (e) 69.6 nm.
- Figure 5.4**.....69  
SEM images and particle size distributions of AuNPs with mean diameters ( $D_{\text{mean}}$ ) of (a) 13.1, (b) 25.2, (c) 37.5, (d) 50.8, and (e) 69.6 nm. Scale bar: 100 nm.
- Figure 5.5**.....70  
Progress curves of the changes in absorption ratios  $A_{620}/A_{\text{peak}}$ , plotted with respect to time in the presence of various concentrations of CRL, after titrating with salt solution. The values of  $A_{\text{peak}}$  of the CRL–AuNP conjugates (UV–Vis spectroscopy) incorporating AuNPs having mean diameters of a) 13.1, b) 25.2, c) 37.5, d) 50.8, and e) 69.6 nm were 520, 524, 530, 534, and 540 nm, respectively.
- Figure 5.6**.....71  
Coverages of the differently sized AuNPs plotted with respect to the CRL concentration. Color scheme: red, green, blue, light blue, and pink represent AuNPs having mean diameters of 13.1, 25.2, 37.5, 50.8, and 69.6 nm, respectively.
- Figure 5.7**.....73  
Schematic representation of the experimental process for the preparation of CRL–AuNP conjugates.
- Figure 5.8**.....73  
Photographic image of the preparation of CRL–AuNP conjugates featuring AuNP sizes varying from 13.1 to 69.6 nm (as shown from left to right in each image). AuNPs with CRL



(a) before and (b) after centrifugation, (c) CRL–AuNP conjugates were washed repeatedly and re-dispersion in PBS solution, (d) CRL–AuNP conjugates with KCN, and (e) CRL–AuNP conjugates with IPA.

**Figure 5.9**.....75  
Photographic images and absorbance spectra of AuNP solutions in different conditions. The AuNP sizes varying from 1 to 5 had the values of absorption peak ( $\lambda_{\text{peak}}$ ) of (a) 518, (b) 522, (c) 527, (d) 531, and (e) 536 nm, respectively.

**Figure 5.10**.....76  
Initial release of *p*NP from *p*NPP, plotted as a function of the reaction time of various CRL–AuNP conjugated systems. Inset: Relative activity. Mean diameters of AuNPs: (a) 13.1, (b) 25.2, (c) 37.5, (d) 50.8, and (e) 69.6 nm.

**Figure 5.11**.....78  
Michaelis–Menten plots for the hydrolyses of *p*NPP mediated by the various functionalized AuNPs. Insets: Initial rates ( $\mu\text{M s}^{-1}$ ) listed with respect to the substrate concentration and the kinetic parameters ( $p < 0.05$ ).

**Figure 5.12**.....79  
Michaelis–Menten plots for *p*NPP hydrolysis catalyzed by CRL–AuNP conjugates featuring AuNP sizes varying from 13.1 to 69.6 nm. Lines of best fit were obtained from the data using Enzyme Kinetics Module software.

**Figure 5.13**.....80  
Plots of the values of (a)  $V_{\text{max}}$  with respect to the enzyme concentration in the presence of various CRL–AuNP conjugate systems and (b)  $K_m$  with respect to the AuNP size.

**Figure 5.14**.....83  
Geometric relationships between the substrate *S*, the enzyme *E* and the nanoparticle *NP*. (a) If the distance between the *S* and *E* was less than the sum of the radii of two bounding spheres,  $r_E + r_S$ , then a collision event occurred. (b) Concerning diffusion effects in a fluid, the effective radius of the enzyme–NP conjugate should increase to  $r_{\text{NP}} + 2r_E$ . (c) The solid-angle fraction  $\Omega$  exposed for collisions between the substrate and the enzyme. (d) Geometric relationships of the respective radii.

## Appendix

### Scheme A1.....98

Flow chart of data processing. It demonstrates the scheme for solving eq (1) to determine the apparent kinetics of immobilized enzyme.

### Table A1.....103

Atomic and structural diffusion volume increments

### Figure A1.....91

Step-by-step and chemical procedures of enzyme immobilization. (a) Process flow showing the samples used and their preparation technique and (b) schematic diagram of the chemical linking method of enzymes CRL binding to the silica substrate.

### Figure A2.....93

CRL-catalyzed hydrolysis reaction and the associated setups of assay systems. (a) *p*NPP was used as substrate for CRL. The common product, *p*NP, which gives strong absorption at 410 nm in neutral or alkaline, served as the reporter molecule for the progress of the enzyme-catalyzed reaction. Schematic diagram of a typical microfluidic-reactor instrument for (b) the CRL assay system with enzyme-free (*via* bypass) as base line; the substrate *S* is *p*NPP,  $[S]_{o,H} = 80 \mu\text{M}$ ,  $[S]_{o,L} = 4 \mu\text{M}$ .

### Figure A3.....99

The typical progress curves of enzymatic assays for immobilized CRL. The absorbance of time courses was obtained after setting zero with no enzyme *via* a bypass in the CRL assay. The breaks in x-axis, progress time *t*, were due to bypass steps.

### Figure A4.....101

Plots of surface-immobilized CRL kinetic data. The typical plots (a) and (b) show the iterative fitting process operated by the set of eqs (4) and (5), respectively. (a) For the solubility limit of substrate *p*NPP in the CRL assay, the initial approximation  $\langle V^*_{max}/H \rangle_0$  (open symbol) were still obtained from eq (2) by linear regression using  $[p\text{NPP}]_{o,H} = 80 \mu\text{M}$ , and fitted to the exponential decay curve (dash-dot-dot). Fitting curves  $r = 1-5$  were corresponding to the five successive approximations of eq (4); the solid symbol means the converged value of  $V^*_{max}/H$  with four significant figures. In fact, the fitting curves  $r = 1$  and  $r = 5$  converged to one curve. (b) The open symbol and solid symbol represent the initial and the fifth approximations of eqs (3) and (5) by linear regression, respectively. The value of

$K_m^*$  of immobilized CRL has converged to 22.09  $\mu\text{M}$  with four significant figures after five successive approximation ( $r = 1-5$ ). (c) The predicted  $K_m^*$  values, the slopes of regression lines fitting lines in eq (5), of immobilized CRL are the result of three set of independent experiment data ( $n = 1-3$ ).



# List of Abbreviations

ATP	adenosine triphosphate
AuNPs	gold nanoparticles
CD	circular dichroism
ChT	$\alpha$ -chymotrypsin
CRL	<i>Candida rugosa</i> lipase
Cy5	cyanine dye 5
DI water	deionized water
DLS	dynamic light scattering
DNA	deoxyribonucleic acid
Fab	antigen-binding fragment
FTIR	fourier transform infrared spectroscopy
IPA	propan-2-ol
IPP	image-pro plus
KCN	potassium cyanide
MMPCs	mixed monolayer protected gold clusters
MPTMS	3-mercaptopropyl-trimethoxy-silane
MRI	magnetic resonance imaging
<i>p</i> NP	<i>p</i> -nitrophenol
<i>p</i> NPP	<i>p</i> -nitrophenyl palmitate
NPs	nanoparticles
SAMs	self-assembled monolayers
SEM	scanning electron microscopy
SPR	surface plasmon resonance
XPS	X-ray photoelectron spectroscopy

# List of Symbols

$v$	reaction rate
$V_{\max}$	maximum velocity
$k_{\text{cat}}$	turnover number
$K_m$	Michaelis constant
$k_{\text{cat}}/K_m$	specificity constant
$E_{\text{NP}}$	enzyme/NP conjugate
$k_{\text{E-NP}}^{\text{coll}}$	bimolecular rate constant
$C_E$	enzyme concentration
$C_S$	substrate concentration
$Z$	frequency of collisions
$p$	fraction of substrates with correct orientation
$E_{\text{act}}$	activation energy
$R$	gas constant
$T$	absolute temperature
$\Omega$	open solid-angle fraction
$\eta$	shielding factor
$r_{\text{NP}}$	NP radii
$r_E$	enzyme radii
$r_S$	substrate radii
$D_E$	enzyme diffusion coefficient
$D_S$	substrate diffusion coefficient
$N_E$	enzyme number concentration
$N_S$	substrate number concentration
$N_{\text{Avo}}$	Avogadro's constant
$k_B$	Boltzmann constant
$\mu$	viscosity of solution
$k_{\max}^{\text{eff}}$	maximum frequency of effective collisions

